HHS Public Access

Author manuscript

Nat Metab. Author manuscript; available in PMC 2019 July 21.

Published in final edited form as:

Nat Metab. 2019 February ; 1(2): 212–221. doi:10.1038/s42255-018-0029-0.

Perineuronal Net Formation during the Critical Period for Neuronal Maturation in the Hypothalamic Arcuate Nucleus

Zaman Mirzadeh[1], **Kimberly M. Alonge**[2], **Elaine Cabrales**[1], **Vicente Herranz-Pérez**[4,5], **Jarrad M. Scarlett**[2,3], **Jenny M. Brown**[2], **Rim Hassouna**[6], **Miles E. Matsen**[2], **Hong T. Nguyen**[2], **Jose Manuel Garcia-Verdugo**[4], **Lori M. Zeltser**[6,7], and **Michael W. Schwartz**[2]

[1]Department of Neurosurgery, Barrow Neurological Institute, Phoenix, AZ, USA.

[2]Diabetes Institute, School of Medicine, University of Washington, Seattle, WA, USA.

[3]Department of Pediatric Gastroenterology and Hepatology, Seattle Children's Hospital, Seattle, WA, USA.

[4]Laboratory of Comparative Neurobiology, Instituto Cavanilles, CIBERNED, Universidad de Valencia, 46980 Valencia, Spain.

[5]Predepartmental Unit of Medicine, Faculty of Health Sciences, Universitat Jaume I, 12071 Castelló de la Plana, Spain.

[6]Naomi Berrie Diabetes Center, Columbia University, New York, NY, USA.

[7]Department of Pathology and Cell Biology, Columbia University, New York, NY, USA.

Summary

In leptin-deficient *ob/ob* mice, obesity and diabetes are associated with abnormal development of neurocircuits in the hypothalamic arcuate nucleus (ARC)[1], a critical brain area for energy and glucose homeostasis[2,3]. As this developmental defect can be remedied by systemic leptin administration, but only if given before postnatal day 28, a critical period (CP) for leptin-dependent development of ARC neurocircuits has been proposed[4]. In other brain areas, CP closure coincides with the appearance of perineuronal nets (PNNs), extracellular matrix specializations that restrict the plasticity of neurons that they enmesh[5]. Here we report that in humans as well as rodents, subsets of neurons in the mediobasal aspect of the ARC are enmeshed by PNN-like structures. In mice, these neurons are densely-packed into a continuous ring that encircles the junction of the ARC and median eminence, which facilitates exposure of ARC neurons to the

*Please address correspondence or materials requests to the Corresponding Authors: Michael W. Schwartz, MD, Professor and RH Williams Endowed Chair in Medicine, Co-Director, Diabetes Institute, University of Washington School of Medicine, 850 Republican Street, Box 358055, Seattle, WA 98109, mschwart@uw.edu, Zaman Mirzadeh, MD PhD, Assistant Professor, Department of Neurosurgery, Barrow Neurological Institute, St. Joseph's Hospital and Medical Center, 350 W. Thomas Rd., Phoenix, AZ 85013, zaman.mirzadeh@barrowneuro.org.

Author Contributions:

conception/design of work: ZM, KMA, MWS, data acquisition/analysis/interpretation: ZM, KMA, EC, VHP, JMS, JMB, RH, MEM, HTN, JMGV, LMZ, MWS, manuscript draft/revisions: ZM, MWS. All authors approved the final version of the manuscript.

Competing Interests Statement

The authors declare no competing financial or non-financial interests in relation to the work described here.

circulation. Most of the enmeshed neurons are both GABAergic and leptin receptor-positive, including a majority of Agrp neurons. Postnatal formation of the PNN-like structures coincides precisely with closure of the CP for Agrp neuron maturation and is dependent on input from circulating leptin, as postnatal *ob/ob* mice have reduced ARC PNN-like material that is restored by leptin administration during the CP. We conclude that neurons crucial to metabolic homeostasis are enmeshed by PNN-like structures and organized into a densely packed cluster situated circumferentially at the ARC-ME junction, where metabolically-relevant humoral signals are sensed.

During critical periods (CPs) of early postnatal life, developing neurocircuits are exquisitely sensitive to and shaped by external cues from the environment[6]. The CP for ocular dominance plasticity in primary visual cortex (V1) is a well-studied example: during the CP, but not before or after, visual deprivation of one eye induces a strong shift of neuronal responses to the non-deprived eye[7]. The associated loss of acuity in the deprived eye, clinically referred to as amblyopia, is difficult to remedy after CP closure.

In diverse neurocircuits ranging from the mammalian visual, barrel (somatosensory) and entorhinal cortices to the hippocampus and amygdala, and in song nuclei in the songbird brain as well, CP closure is dependent on the formation of perineuronal nets (PNNs)[5,8–14]. PNNs are a specialized, condensed form of extracellular matrix (ECM), composed largely of hyaluronan and chondroitin sulfate proteoglycans, arranged in lattice-like structures that enmesh the soma and proximal dendrites of subsets of neurons, primarily inhibitory interneurons[9,15]. Remarkably, experimentally disrupting PNNs in adult animals is capable of reactivating CP plasticity in these diverse brain areas. In V1, for example, PNN digestion enables restoration of vision to a previously deprived eye[5]. Comparable restorative effects of PNN disruption are reported across neurological and psychiatric disorders as diverse as PTSD, depression, drug addiction and spinal cord injury[9,15].

Recently, compelling evidence was provided in support of the existence of a CP for the maturation of Agouti-related peptide (Agrp) neurons in the hypothalamic arcuate nucleus (ARC)[4]. As key regulators of feeding behavior, Agrp neurons are among the best-studied of all hypothalamic neurons. These GABAergic neurons co-express the potent orexigen neuropeptide Y (NPY), and they project to downstream targets in homeostatic circuits governing energy balance and glucose homeostasis. Maturation of these projections occurs during the lactation period, concomitant with a naturally-occurring leptin surge (P4–P14)[1,16], and this maturation process appears to be dependent on leptin since these projections fail to develop properly in leptin-deficient *ob/ob* mice (a genetic model of obesity and type 2 diabetes (T2D)). Moreover, this defect in Agrp neuron development can be rescued by treatment with exogenous leptin, but only if administered before P28[1,4]. A CP for the trophic action of leptin on Agrp neuron maturation therefore exists, and its closure coincides with both the transition to independent feeding and maturation of the cellular response of Agrp neurons to input from leptin[17]. This CP is also a uniquely sensitive time when both over- and undernutrition predispose to obesity and glucose intolerance in adulthood[18–22].

Here we show that key subpopulations of ARC neurons are enmeshed by PNN-like material in humans as well as rodents. These neurons are predominantly GABAergic and many are leptin-receptor positive, including a majority of Agrp neurons. These enmeshed neurons are organized into a densely packed ring that delimits the junction of the ARC and median eminence (ME), a circumventricular organ (CVO) that provides hypothalamic neurons with access to hormones and nutrients in the circulation. Moreover, the postnatal appearance of these PNNs both coincides with closure of the CP for Agrp neuron development and is dependent upon input from leptin.

Since PNN-enmeshed neurons in other brain areas are not tightly packed, nor are they concentrated near CVOs or regulated by circulating signals, the anatomical arrangement we report here appears to be unique. Nevertheless, based on our findings that the condensed ECM material that enmeshes neurons at the ARC-ME junction is both biochemically and ultrastructurally indistinguishable from PNNs in other brain areas, we refer to them as "PNNs" (rather than "PNN-like structures").

We performed immunohistochemistry (IHC) on serial coronal sections of mouse hypothalamus using *Wisteria floribunda* agglutinin, a lectin that selectively labels the *N*-acetylgalactosamine residue on chondroitin sulfate (CS) chains in PNNs. Our initial survey (Supplementary Figure 1) revealed numerous PNN-enmeshed cells localized to the junction of the ARC and median eminence (ME) (Figure 1a–d). Compared to the rather sparse distribution of PNN-enmeshed neurons in most brain areas (*e.g.*, V1), enmeshed cells in the ARC-ME area are densely packed (Figure 1e, g). To better characterize the structural features of these cells, we used high-resolution confocal microscopy combined with Imaris image analysis of individually-labelled, PNN-enmeshed neurons located at the periphery of the dense cluster at the ARC-ME junction. Analysis of these cells (**arrow f in** Figure 1c) allowed us to better define the anatomical relationship between PNNs and the neurons they enmesh without the confounding influence of labeling on an adjacent, closely apposed cell. As expected, PNNs enwrap both cell soma and proximal processes (Figure 1f), reminiscent of PNN structures described in the visual cortex (Figure 1g,h). Wholemount preparations of the mediobasal hypothalamus, stained with WFA and imaged from either the ventricular surface (Figure 1i) or the ventral pial brain surface (Figure 1j), revealed the presence of a continuous "collar" of PNN-enmeshed cells at the junction of the ARC and ME.

As a first step to determine if these ARC WFA-labeled structures are *bone fide* PNNs, we micro-injected 10 milliunits of Chondroitinase ABC (ChABC), an enzyme that digests PNNs, stereotactically into the ARC of wild-type mice. Subsequent histochemical analysis of these animals (n=3) revealed ChABC-mediated digestion of ARC-ME PNNs on the injected side (Figure 1k). Then, following a previously validated protocol[23], we performed pre-embedding WFA-DAB labeling of mouse brain sections for study by electron microscopy. This ultrastructural analysis revealed DAB electron-dense deposits surrounding the soma (Figure 1m white arrowheads) and neurites (Figure 1m white arrows) of ARC neurons in a distribution that closely matches the pattern observed in PNN-enmeshed cells in the cortex and hippocampus (Supplementary Figure 2).

In addition to chondroitin sulfate (CS) carbohydrate chains labeled by WFA, PNNs are comprised of two other major components: the CS proteoglycan (CSPG) core proteins to which the CS chains covalently bind, and hyaluronic acid (HA), a long carbohydrate polymer to which CSPG core proteins noncovalently bind. Using biotinylated-HA-binding protein (HABP)[24], we histochemically stained HA in the hypothalamus. Although HABP lightly stains the extracellular matrix throughout brain parenchyma, we observed an increased abundance of HA that colocalizes with WFA at the junction of the ARC and ME (Figure 1o and Supplementary Figure 3), confirming that WFA (+) structures in this brain area contain HA. To identify the relevant CSPG(s) present in these PNNs, we next stained for each of the 5 major CSPG species found in PNNs elsewhere in the brain: aggrecan, brevican, neurocan, versican and phosphacan. Interestingly, although each of these CSPGs was detected in various mouse brain areas (data not shown), only phosphacan (PCAN) immunoreactivity was co-localized with WFA in mouse ARC-ME (Figure 1p and Supplementary Figure 3).

We also immunostained for CD44, the cell surface receptor for HA, and found that its expression in this brain area is largely limited to tanycytes, with high expression localized to E3/β-tanycytes piercing through the PNN domain and little to no expression in dorsal E2/α-tanycytes that circumvented the PNN domain (Supplementary Figure 4b, c). An IHC survey of CD44 expression in serial coronal sections through the hypothalamus revealed a striking colocalization with the PNN domain in the ventromedial ARC (Supplementary Figure 4a). These findings raise the possibility that via activation of CD44, signal transduction in tanycytes is evoked by HA present in PNNs.

The ARC is uniquely specialized to sense and transduce input from nutritionally-relevant hormones (such as leptin and insulin) and nutrients (*e.g.*, glucose, free fatty acids and amino acids) into adaptive changes of food intake and energy metabolism[2]. Among key neuronal subsets implicated in this homeostatic circuitry are Agrp and pro-opiomelanocortin (Pomc) neurons, with the former being GABAergic[25]. To identify distinct ARC neuronal subtypes that are among those enmeshed by PNNs (= # neurons of particular subtype / total # PNN-enmeshed cells), we performed IHC on coronal sections from transgenic mouse lines that provided whole cell GFP-filling. Using GAD67-GFP heterozygous knock-in mice, we confirmed that a vast majority of ARC neurons enmeshed by PNNs are GABAergic (81.8 ± 0.7% of ARC PNN-enmeshed cells; n=3 GAD67-GFP mice; note that dots in dot plots throughout this work represent data from independent animals) (Figure 2a–d), as is the case for PNN-enmeshed neurons in other brain areas[9]. Three-dimensional reconstruction of GAD67-GFP+ PNN-enmeshed cells (Supplementary Movie 1) revealed PNN enmeshing the soma and proximal dendrites of GABAergic ARC cells in a manner comparable to that of GABAergic interneurons in V1, with some differences in morphology due likely to differences in cell type and process ramification (Supplementary Figure 5 and Supplementary Movie 2).

To determine if ARC neurons that express leptin receptors are represented among those enmeshed by PNNs, we employed Leptin Receptor b-Cre;Ai14 td-Tomato reporter mice to histochemically identify leptin-receptor positive cells. These cells comprised 81.7 ± 1.5% of all PNN-enmeshed cells in the ARC (n=3 LepRb-Cre;Ai14) (Figure 2e–g). To identify Agrp

neurons, we used NPY-GFP transgenic mice (since NPY and Agrp are expressed in the same ARC neuronal subset) and found that these cells (which are GABAergic, and many of which express leptin receptors) also account for a majority of ARC PNN cells (58.5 ± 1.0%; n=3 NPY-GFP mice) (Figure 2h–j and Supplementary Movie 3). By comparison, POMC neurons comprised a much smaller fraction of PNN-enmeshed cells in this brain area (13.7 ± 2.3%; n=3 POMC-GFP mice) (Figure 2k–m).

A separate but related question pertains to the fraction of Agrp or POMC neurons in the ARC that are enmeshed by PNNs (= # PNN-enmeshed neurons of particular subtype / total # neurons of that subtype). As predicted, the fraction of Agrp neurons enmeshed by PNNs (78.3 ± 1.7% NPY-GFP neurons) is greater than the fraction of POMC neurons (43.6 ± 3.3% POMC-GFP neurons). A third peptidergic cell type found in the ARC expresses somatostatin (SST), which is challenging to detect histochemically because the SST peptide is rapidly exported from soma into axons. To address this issue, we administered a single intracerebroventricular (ICV) injection of colchicine to wild-type mice, which prevents transport of SST out of the soma and thus enables somatic labeling with SST antibodies. We report that while this approach allowed us to identify ample SST+ soma, few of these were PNN-enmeshed (1.2 ± 0.6%; n=3) (Figure 2n–o). As confirmation of the efficacy of ICV colchicine to prevent neuropeptide export from the soma, we note that many Agrp+ PNN-enmeshed cell bodies were also observed, corroborating our findings in NPY-GFP mice (Figure 2o). Together, these findings indicate that only a subset of ARC neurons – specifically, those neurons most closely linked to control of energy balance and metabolic homeostasis – are enmeshed by PNNs.

A key question raised by these observations is whether PNNs contribute to closure of the CP for ARC neurocircuit development, as is true of V1 and other brain areas. As a first step to address this question, we performed a developmental time-series analysis of PNN formation over the lactation and periweaning period from postnatal day 10 (P10) to P30 in wildtype mice (Figure 3). This approach was based on evidence that leptin-dependent maturation of ARC-ME neurocircuits occurs during a CP that closes ~P28[1,4], so PNNs must appear during this period if they are to contribute to closure of this CP. WFA labeling revealed only a very faint signal at P10 (10.0 ± 0.8 intensity units; n=4 C57B/6 mice) that lacked the typical PNN honeycomb configuration (Figure 3a). By P21, WFA labeling intensity had increased by more than 2-fold (27.4 ± 1.7 intensity units; n=5 mice) and structural features of PNNs were evident (Figure 3b). WFA intensity was further increased at P30 (46.2 ± 2.6 intensity units; n=3 mice), by which time PNN structures appeared fully formed (Figure 3c).

The time course of ARC PNN formation during postnatal development in wildtype mice was closely paralleled by the maturation of Agrp neuron projections, quantified as an increase in Agrp fiber density in the ARC (0.23 ± 0.07% at P10; 0.87 ± 0.11% at P21; 1.48 ± 0.14% at P30) (Figure 3d). We note that at CP closure (~P28), both PNNs and Agrp fiber density in the ARC were transiently increased over values characteristic of adult mice (P90: WFA 34.1 ± 2.5 intensity units; Agrp fiber density 1.05 ± 0.09%). During postnatal development, the domain of CD44 expressing tanycytes also expanded from medial (where it covered only the ME β-tanycytes at P21) to lateral and dorsal along the ventricular lining, paralleling the

progressive appearance of PNNs (Supplementary Figure 4d,e; compare yellow and white arrows and arrowheads).

The tight temporal association between ARC PNN formation and maturation of Agrp neuron projections coincides closely with closure of the CP for Agrp neuron development (~P28)[4]. Given the key role played by leptin in the latter process, we next sought to investigate whether input from leptin influences ARC PNN formation. To this end, we performed a developmental time-series analysis of ARC WFA labeling in *ob/ob* pups and *ob/+* control littermates at P15, P21, and P30. At each of these ages, we found that in *ob/ob* mice, ARC WFA intensity (normalized to the mean value of control littermates) was significantly below that detected in controls (*P15*: 0.92 ± 0.01, n=3 *ob/ob* vs. 1.00 ± 0.00, n=2 *ob/+*, p=0.002; *P21*: 0.89 ± 0.01, n=5 *ob/ob* vs. 1.00 ± 0.02, n=5 *ob/+*, p=0.0005; *P30*: 0.87 ± 0.01, n=5 *ob/ob* vs. 1.00 ± 0.00, n=5 *ob/+*, p<0.0001) (Figure 4a–d, g).

Based on these results, we hypothesized that like Agrp neuron maturation, formation of PNNs in the ARC is dependent on input from circulating leptin. To test this hypothesis, we administered either leptin or vehicle to *ob/ob* pups according to a schedule reported to mimic the postnatal leptin surge that was used to define the CP for Agrp neuron maturation[4]. Specifically, *ob/ob* pups received a daily intraperitoneal injection of either leptin (10 mg/kg) or vehicle from P10 to P30, and were euthanized one day later for IHC analysis. As predicted, ARC WFA intensity was significantly increased in leptin- compared to vehicle-treated *ob/ob* pups (*P30 rescue*: 1.15 ± 0.02, n=3 *ob/ob-leptin* vs. 1.00 ± 0.01, n=2 *ob/ob-vehicle*, p=0.02) (Figure 4e, f, h). There was no significant difference in weight gain between the leptin and vehicle-treated groups. Interestingly, the presence of Agrp+ soma in the ARC of vehicle-treated pups, but not leptin-treated pups (insets in Figure 4e, f) appears to offer confirmatory evidence of leptin action, which is known to reduce Agrp expression[26]. A similar pattern was also observed when Agrp staining between *ob/+* and *ob/ob* pups was compared at P30 (insets in Figure 4c, d).

To determine how ARC PNNs are affected by persistent leptin deficiency in adulthood, we performed WFA labeling of 12 week-old *ob/ob* mice and age-matched C57B/6 mice followed by high-resolution confocal microscopy and Imaris 3-dimensional image analysis (Supplementary Figure 6a, b). Paradoxically, in the ARC-ME area, WFA intensity in *ob/ob* mice (normalized to the mean value of age-matched controls) was significantly higher than in controls (1.24±0.05, n=5 *ob/ob* vs. 1.00±0.03, n=5 wt; p=0.004) (Supplementary Figure 6e), whereas no such difference in intensity was detected in primary visual cortex of the same animals (1.00±0.01, n=5 *ob/ob* vs. 0.99±0.01, n=5 wt; p=0.2) (Supplementary Figure 7, note that ARC WFA intensity data shown in Supplementary Figure 7 are replicated from the left panel in Supplementary Figure 6e in order to make two different points—comparing ARC WFA to ARC CD44 intensity in Supplementary Figure 6e and comparing ARC WFA to V1 WFA intensity in Supplementary Figure 7). To investigate whether this increase of ARC PNN intensity in *ob/ob* mice was the result of leptin deficiency or was instead secondary to obesity, we compared WFA staining intensity between cohorts of wild-type C57B/6 mice that were either made obese through high-fat diet (HFD) feeding for 12 weeks (beginning at age 12 weeks) or were fed standard chow and sacrificed at the same age. We report that whereas no difference in ARC WFA intensity was detected between HFD and

chow-fed cohorts (1.00±0.00, n=5 hfd vs. 1.00±0.00, n=3 chow), tanycytic CD44 expression was increased in the former group (1.11±0.03, n=5 hfd vs. 1.00±0.01, n=5 chow; p=0.007) (Supplementary Figure 6c–e). In contrast, no difference in tanycytic CD44 expression was observed between *ob/ob* and chow-fed control mice (1.01±0.03, n=5 *ob/ob* vs. 1.00±0.03, n=5 wt; p=0.8). Together, these data suggest that increased PNN intensity in the ARC of adult *ob/ob* mice is secondary to leptin deficiency rather than to obesity *per se*, whereas the reverse is true for the increase of tanycytic CD44 expression in HFD-fed (but not *ob/ob)* mice.

To determine if PNNs are present in the ARC of other mammalian species, we performed WFA staining in the hypothalamus of both rats and humans. We report that PNNs are present in the ARC-ME of all 3 species (Supplementary Figures 8 and 9). As in the mouse, a majority of cells enmeshed by PNNs in the human ARC are NPY/Agrp neurons, with both the soma and proximal dendrites of these neurons wrapped by WFA+ material (Supplementary Figure 8 and Supplementary Movie 4). Interestingly, PNN-enmeshed cells in humans are more sparsely distributed than those in mice, which enhances the ability to see how the mesh structure associates with the neuronal contours.

In summary, we report that PNNs enmesh Agrp and other leptin receptor-expressing neurons in the ARC (most of which are GABAergic, similar to neurons enmeshed by PNNs in visual cortex and other brain areas), and that their appearance during postnatal development coincides closely with both maturation of Agrp neuron projections and closure of the CP for leptin-mediated regulation of Agrp neuron development[4]. Situated at the junction of the ARC and ME, these PNNs are detected in humans as well as rodents, and their formation appears to be sensitive to input from leptin, being deficient in the ARC of postnatal *ob/ob* mice, and restored by leptin administration to *ob/ob* mice during the CP. Unlike PNN-enmeshed neurons in other brain areas that tend to be sparsely distributed, these neurons form a densely packed ring that circumscribes the ME—a CVO that facilitates processing of metabolically-relevant humoral input—at its junction with the ARC. Together, these findings describe an apparently unique brain structure that is implicated in closure of the CP for the development of neurocircuits crucial to control of energy balance and glucose metabolism in adulthood. Our findings also suggest that leptin regulation of ARC neuron development during the CP involves an action on PNN formation.

In sharp contrast to the deficiency of PNNs we observed in the ARC during postnatal development, adult *ob/ob* mice exhibit an overabundance of ARC PNNs. To explain this paradoxical finding, we draw upon both *in vivo*[8,27,28] and *in vitro*[29] evidence that PNN formation is driven by activity of the enmeshed neuron. Thus, leptin induces depolarization and increases the excitability of Agrp neurons during the CP (prior to ~p21–23)[17], so leptin action on these neurons may constitute a stimulus to PNN formation during this time. During subsequent development, however, a progressive increase in the expression of ATP-sensitive potassium channels by Agrp neurons leads to a “phenotype switch”, whereby leptin now exerts the hyperpolarizing effect characteristically observed in adult Agrp neurons[17]. Consequently, Agrp neuron activity is predicted to be reduced in leptin-deficient mice during the CP, but increased in adulthood, and PNN formation parallels these changes.

Available evidence suggests both that ARC neurocircuits are highly plastic during development and that this plasticity is markedly reduced upon CP closure. Thus, whereas Agrp neuron ablation induces life-threatening starvation when it occurs in adult mice, it has little or no phenotypic impact when induced shortly after birth[30]. Similarly, CRISPR-mediated deletion of leptin receptors selectively from Agrp neurons in adults recapitulates most of the phenotype of whole body leptin deficiency (hyperphagia, obesity and diabetes), whereas the same deletion has little detectable effect when induced during development[31]. Combined with evidence that over the course of the CP, when Agrp neurons innervate their downstream targets[1,4], their response to leptin switches from excitatory to inhibitory[17], these data collectively point to the existence of a mechanism whereby Agrp-linked circuit plasticity during postnatal development is sharply constrained in adulthood. PNNs are likely candidates to mediate this effect, as they can limit plasticity both through direct signaling effects of CSPGs on the enmeshed neuron and by providing a scaffold for binding regulatory molecules such as Otx2[13] (which suppresses plasticity) and the chemorepulsive molecule Semaphorin 3a[32] (which promotes growth of projections away from the enmeshed neuron)[5,8–14,32].

Such a role for PNNs has important implications for understanding how nutritional excess during postnatal development affects ARC neurocircuits in ways that can predispose to obesity and T2D in adulthood[2]. Specifically, over-nutrition during lactation, due either to maternal HFD consumption[18,20–22] or to culled litter size[19], *1)* reduces numbers of ARC neurons expressing leptin receptors. *2)* decreases leptin responsiveness of these neurons[18,19], 3*)* impairs formation of ARC projections within hypothalamic feeding circuits[18,20], and 4*)* predisposes to excess body adiposity and metabolic dysregulation in adulthood[20–22]. Similarly, epidemiological evidence suggests that in humans, late gestation and early childhood are particularly sensitive periods when environmental exposures can shape a predisposition to metabolic disease in adulthood[33]. Interestingly, early gestational undernutrition is also reliably associated with an increased risk of adult obesity[34,35], and this effect can be partially reversed by leptin treatment during the lactation period[36]. Since PNNs sharply limit the plasticity of neurons that they enmesh, and since elsewhere in the brain, the developmental appearance of PNNs heralds CP closure[37], we interpret our discovery that ARC neurons become enmeshed by PNNs at a time corresponding to CP closure as being of potential relevance to experience-dependent plasticity in neurocircuits for energy balance and glucose homeostasis. It is possible, for example, that experimental re-activation of ARC plasticity in adults will ameliorate metabolic dysfunction, as has been observed following re-induction of plasticity in the visual cortex in models of amblyopia[5].

In addition to limiting plasticity during development, PNNs can be altered in adulthood in ways that impact the function of the neurons they enmesh, and the variable effect of different CSPGs, hyaluronan and other PNN components to influence plasticity is well-documented[37]. PNN composition can also change in response to injury, inflammation, or neurodegeneration in ways that further restrict the plasticity of enmeshed neurons[9]. Thus, either a deficiency[38,39] or an overabundance[9] of PNNs or individual PNN components can have deleterious effects on circuit behavior and neurological function. As one example, functional recovery after spinal cord injury is limited by “strengthening” of PNNs owing to inflammation and reactive gliosis, such that recovery is improved by PNN disruption[37].

In this context, it is notable that diet-induced obesity (DIO) induced by HFD feeding is associated with reactive gliosis involving activation of both microglia and astrocytes in the same ARC area where PNNs are found[40], and recent work suggests that these glial responses are both necessary and sufficient for obesity in this setting[41,42]. In this context, our finding of increased tanycyte expression of the hyaluronan receptor CD44 in mice with DIO is of interest because it raises the possibility that environmental exposures in adulthood (*e.g.*, consuming a HFD) can influence signaling between PNN constituents (*e.g.*, hyaluronan) and adjacent cells (*e.g.*, tanycytes) in the ARC-ME. Reports that tanycytes transport circulating leptin into the mediobasal hypothalamus[43] heighten the potential importance of such interactions. That this obesity-associated increase of tanycyte CD44 content is not observed in *ob/ob* mice despite their severe obesity phenotype is consistent with evidence that hypothalamic gliosis is also not observed in these animals[44], presumably reflecting the requirement for an intact leptin signal in this response.

In conclusion, we report that the ARC-ME junction, a brain area that specializes in processing humoral input relevant to fuel homeostasis, is marked by a cluster of tightly packed, PNN-enmeshed neurons, including a majority of Agrp neurons. The formation of these PNNs coincides with closure of the CP for ARC neuron development and, like postnatal maturation of Agrp neurons, is dependent on input from the adipocyte hormone leptin. Future investigation is needed to clarify the extent to which both PNN composition and ARC neuronal plasticity are altered in models of obesity, diabetes and related metabolic disorders, and whether PNN formation in this region can be altered pharmacologically.

Methods

Animals

GAD67-GFP knock-in[45], LepRb-Cre;Ai14 reporter[46,47], Npy-GFP[48], POMC-GFP[49], and wild-type C57B/6 mice (Jackson Labs), age P60 to P120, were used to characterize neuronal and glial subtypes associated with ARC PNNs. Wild-type C57B/6 mice, age P0 to P90 were used for developmental time-series studies to characterize PNN formation and Agrp neuron maturation. To study the effects of leptin deficiency on PNN formation, we used *ob/ob* mice and their *ob/+* littermate controls (Jackson Labs). To characterize PNNs in rats, we used the Wistar strain (Harlan). Both sexes were used for all studies. Mice were on 12h:12h light-dark cycle in 5/cage group housing. Animals were perfusion-fixed with saline and 4% paraformaldehyde (PFA), the brains were extracted, post-fixed overnight at 4°C, then sectioned using a vibratome (50 um) or cryostat (12 um). The Institutional Animal Care and Use Committees at St. Joseph's Hospital and Medical Center and the University of Washington approved all animal procedures. All animal studies were conducted in compliance with the relevant ethical regulations.

Human Specimens

Three brains (ages 23, 64, and 71 years with postmortem intervals 8, 9, and 12 hours, respectively) were collected at autopsy. Multiple wholemount blocks were dissected from the hypothalamus along the 3rd ventricle from each brain, their positions along the 3rd ventricle wall were documented, and the tissue was immersion-fixed in 4% PFA at 4°C for

24 hours. All specimens were collected with informed consent and in ethical compliance with the St. Joseph's Hospital and Medical Center Committee on Human Research (IRB approval no. 10BN159).

Stereotactic Intracranial Injections

Animals were head-fixed with ear bars in a custom digital stereotactic rig used to perform unilateral intra-ARC injections of Chondroitinase ABC (10 milliunits in 100 nanoliters sterile PBS) at the coordinates (0.3 mm lat, 1.1 mm posterior, 5.6 mm depth) relative to bregma, and sacrificed 48h later. For ICV colchicine administration, 1 ul of colchicine (10 ug/ul in sterile PBS) was injected at (1.3, 0, 1.5) relative to bregma and animals were sacrificed 24h later.

Postnatal leptin administration

We crossed ob/+ mice to generate litters containing *ob/ob* pups. Litters were genotyped at P1–2 and litter sizes were adjusted to 6–8 pups to standardize nutrition during lactation period. Leptin (10 mg/kg i.p.; made available via Dr. A.F. Parlow; National Hormone & Peptide Program, CA) or vehicle was administered to *ob/ob* littermates on a daily basis at noon from P10-P30 and the animals were euthanized 24 hours after the last injection.

Wholemount Dissection

After cervical dislocation, the mouse brain was removed from the skull and 3V wholemounts were freshly dissected using principles similar to those described for LV wholemounts[50]. Briefly, 3V wholemounts were dissected by performing a ventriculotomy of the 3V from ventral to dorsal and rostral to caudal. The exposed ventricle walls were immersion-fixed in 4% PFA at 4°C overnight prior to immunostaining.

Immunohistochemistry and Microscopy

For *Wisteria Floribunda* agglutinin (1:500, Sigma L1516) or HA-binding protein (1:50, AMSbio AMS.HKD-BC41) staining, sections were incubated in WFA or HABP in PBS with 0.5% TX followed by streptavidin-Alexa 488 or 561 (1:1000, Invitrogen Molecular Probes) in PBS/0.5% TX, each for 24h at 4°C. For immunostaining, sections were incubated in primary and secondary antibodies in PBS/0.5% TX and 5% normal goat serum for 24–48h at 4°C. Primary antibodies: chicken anti-GFP (1:500, Aves Labs GFP-1020), rabbit anti-dsRed (1:1000, Clontech 632496), rabbit anti-Agrp (1:200, Phoenix Pharmaceuticals H-003–57), rabbit anti-Npy (1:1000, Abcam ab30914), rat anti-somatostatin (1:500, EMD Millipore MAB354), chicken anti-vimentin (1:500, EMD Millipore AB5733), rabbit anti-CD44 (1:1000, Abcam ab157107), and rat anti-phosphacan DSD-1 (1:500, EMD Millipore MAB5790-I). Secondary antibodies: conjugated to Alexa Fluor dyes (goat or donkey polyclonal, 1:500, Invitrogen). Confocal images were taken on a Leica SPE.

Electron Microscopy

Adult C57B/6 mice (Jackson Labs) were transcardially perfused with 4% PFA and 0.5% glutaraldehyde (EMS) in 100 mM phosphate buffer (PB). Brains were post-fixed at 4°C overnight, and 50 μm coronal sections were cut on a Leica VT1000 S vibratome. Pre-

embedding IHC was performed using WFA (Sigma L1516), amplified with Vectastain Elite ABC kit (Vector Laboratories), and developed with DAB[23]. Sections were postfixed in 1% osmium tetroxide for 30 min and then embedded in Durcupan ACM epoxy resin (Fluka, Sigma-Aldrich)[51]. For reconstruction of WFA-labeled neurons, we cut ~200 serial semithin (1.5 μm) sections on an Ultracut UC-6 ultramictrotome. Selected semithin sections were glued to resin blocks and detached from glass slides by repeated freeze-thaw. Ultrathin sections (60–80 nm) were then cut and placed on Formvar-coated single-slot grids, stained with lead citrate, and examined at 80 kV on a FEI Tecnai G2 Spirit transmission electron microscope equipped with a Morada CCD digital camera (Olympus).

Image Analysis and Quantification

To quantify the proportion of various ARC neuronal subtypes enmeshed by PNNs, we used high resolution confocal z-stacks to reconstruct the ventromedial arcuate region containing PNN structures in two coronal sections containing the median eminence (Bregma −1.7 and −2.0). Only reporter-labelled cells that were completely enmeshed (360°) by WFA-labelled PNN matrix were counted as positive. To analyze the intensity of WFA or CD44 labeling, high resolution confocal z-stacks were volumetrically analyzed in Imaris image analysis software (Bitplane) and voxel intensities throughout the region of interest (e.g. Arc) were determined (intensity unit range, 0–255) and compared across study groups. Raw images were then rendered as 3-dimensional spectral images corresponding to individual voxel intensities. For Agrp fiber density measurements, we used Imaris software to determine the volume of Agrp-labeled positive voxels, above a set intensity threshold, as a fraction of the total volume in the measured region of interest.

Statistical Analysis

Descriptive statistics and two-tailed t-tests were computed in GraphPad Prism 7. P-value less than 0.05 was considered statistically significant. Unless otherwise stated, dot plots show dots representing data from independent animals with mean and standard error of the mean shown as bars.

Supplementary Material

Refer to Web version on PubMed Central for supplementary material.

Acknowledgements:

The authors are grateful to the original providers of the transgenic mouse lines used in this work: Nobuaki Tamamaki (GAD67-GFP), Martin Myers (LepRb-Cre), Hongkui Zeng (Ai14), Bradford Lowell (Npy-GFP), and Malcolm Low (POMC-GFP). This work was supported by the US NIH National Institute of Diabetes and Digestive and Kidney Diseases (grant nos. DK108596 (Z.M.), DK114474 (J.M.S.), DK083042 (M.W.S.), DK090320 (M.W.S.), and DK101997 (M.W.S.)), National Institute of Neurological Disorders and Stroke Neurosurgeon Research Career Development Program K Award (Z.M.), the American Diabetes Association (grant no. 7–11-BS-179 (L.Z.)), the Russell Berrie Foundation (R.H.), and the Barrow Neurological Foundation (Z.M.).

Data Availability Statement

The data that support the findings of this study are available from the corresponding authors upon request. Additional detailed information on experimental design and reagents is available in the Reporting Summary.

References

1. Bouret SG, Draper SJ & Simerly RB Trophic action of leptin on hypothalamic neurons that regulate feeding. Science 304, 108–110, doi:10.1126/science.1095004 (2004). [PubMed: 15064420]
2. Schwartz MW et al. Obesity Pathogenesis: An Endocrine Society Scientific Statement. Endocr Rev 38, 267–296, doi:10.1210/er.2017-00111 (2017). [PubMed: 28898979]
3. Deem JD, Muta K, Scarlett JM, Morton GJ & Schwartz MW How Should We Think About the Role of the Brain in Glucose Homeostasis and Diabetes? Diabetes 66, 1758–1765, doi:10.2337/dbi16-0067 (2017). [PubMed: 28603139]
4. Kamitakahara A, Bouyer K, Wang CH & Simerly R A critical period for the trophic actions of leptin on AgRP neurons in the arcuate nucleus of the hypothalamus. J Comp Neurol 526, 133–145, doi:10.1002/cne.24327 (2018). [PubMed: 28891045]
5. Pizzorusso T et al. Reactivation of ocular dominance plasticity in the adult visual cortex. Science 298, 1248–1251, doi:10.1126/science.1072699 (2002). [PubMed: 12424383]
6. Hensch TK Critical period plasticity in local cortical circuits. Nat Rev Neurosci 6, 877–888 (2005). [PubMed: 16261181]
7. Wiesel TN & Hubel DH Single-Cell Responses in Striate Cortex of Kittens Deprived of Vision in One Eye. J.Neurophysiol. 26, 1003–1017 (1963). [PubMed: 14084161]
8. Carulli D et al. Animals lacking link protein have attenuated perineuronal nets and persistent plasticity. Brain 133, 2331–2347, doi:10.1093/brain/awq145 (2010). [PubMed: 20566484]
9. Kwok JC, Dick G, Wang D & Fawcett JW Extracellular matrix and perineuronal nets in CNS repair. Dev Neurobiol 71, 1073–1089, doi:10.1002/dneu.20974 (2011). [PubMed: 21898855]
10. Balmer TS, Carels VM, Frisch JL & Nick TA Modulation of perineuronal nets and parvalbumin with developmental song learning. J Neurosci 29, 12878–12885, doi:10.1523/JNEUROSCI.2974-09.2009 (2009). [PubMed: 19828802]
11. Gogolla N, Caroni P, Luthi A & Herry C Perineuronal nets protect fear memories from erasure. Science 325, 1258–1261, doi:10.1126/science.1174146 (2009). [PubMed: 19729657]
12. Nowicka D, Soulsby S, Skangiel-Kramska J & Glazewski S Parvalbumin-containing neurons, perineuronal nets and experience-dependent plasticity in murine barrel cortex. The European journal of neuroscience 30, 2053–2063, doi:10.1111/j.1460-9568.2009.06996.x (2009). [PubMed: 20128844]
13. Beurdeley M et al. Otx2 binding to perineuronal nets persistently regulates plasticity in the mature visual cortex. J Neurosci 32, 9429–9437, doi:10.1523/JNEUROSCI.0394-12.2012 (2012). [PubMed: 22764251]
14. Miyata S, Komatsu Y, Yoshimura Y, Taya C & Kitagawa H Persistent cortical plasticity by upregulation of chondroitin 6-sulfation. Nat Neurosci 15, 414–422, S411–412, doi:10.1038/nn.3023 (2012). [PubMed: 22246436]
15. Maeda N Structural variation of chondroitin sulfate and its roles in the central nervous system. Cent Nerv Syst Agents Med Chem 10, 22–31 (2010). [PubMed: 20236040]
16. Ahima RS, Prabakaran D & Flier JS Postnatal leptin surge and regulation of circadian rhythm of leptin by feeding. Implications for energy homeostasis and neuroendocrine function. The Journal of clinical investigation 101, 1020–1027, doi:10.1172/JCI1176 (1998). [PubMed: 9486972]
17. Baquero AF et al. Developmental switch of leptin signaling in arcuate nucleus neurons. J Neurosci 34, 9982–9994, doi:10.1523/JNEUROSCI.0933-14.2014 (2014). [PubMed: 25057200]
18. Bouret SG et al. Hypothalamic neural projections are permanently disrupted in diet-induced obese rats. Cell metabolism 7, 179–185, doi:10.1016/j.cmet.2007.12.001 (2008). [PubMed: 18249177]
19. Glavas MM et al. Early overnutrition results in early-onset arcuate leptin resistance and increased sensitivity to high-fat diet. Endocrinology 151, 1598–1610, doi:10.1210/en.2009-1295 (2010). [PubMed: 20194730]
20. Vogt MC et al. Neonatal insulin action impairs hypothalamic neurocircuit formation in response to maternal high-fat feeding. Cell 156, 495–509, doi:10.1016/j.cell.2014.01.008 (2014). [PubMed: 24462248]

21. Bayol SA, Simbi BH & Stickland NC A maternal cafeteria diet during gestation and lactation promotes adiposity and impairs skeletal muscle development and metabolism in rat offspring at weaning. J Physiol 567, 951–961, doi:10.1113/jphysiol.2005.088989 (2005). [PubMed: 16020464]
22. Gorski JN, Dunn-Meynell AA, Hartman TG & Levin BE Postnatal environment overrides genetic and prenatal factors influencing offspring obesity and insulin resistance. Am J Physiol Regul Integr Comp Physiol 291, R768–778, doi:10.1152/ajpregu.00138.2006 (2006). [PubMed: 16614055]
23. Carstens KE, Phillips ML, Pozzo-Miller L, Weinberg RJ & Dudek SM Perineuronal Nets Suppress Plasticity of Excitatory Synapses on CA2 Pyramidal Neurons. J Neurosci 36, 6312–6320, doi: 10.1523/JNEUROSCI.0245-16.2016 (2016). [PubMed: 27277807]
24. Koppe G, Bruckner G, Hartig W, Delpech B & Bigl V Characterization of proteoglycan-containing perineuronal nets by enzymatic treatments of rat brain sections. Histochem J 29, 11–20 (1997). [PubMed: 9088941]
25. Backberg M, Collin M, Ovesjo ML & Meister B Chemical coding of GABA(B) receptor-immunoreactive neurones in hypothalamic regions regulating body weight. J Neuroendocrinol 15, 1–14 (2003). [PubMed: 12535164]
26. Morrison CD, Morton GJ, Niswender KD, Gelling RW & Schwartz MW Leptin inhibits hypothalamic Npy and Agrp gene expression via a mechanism that requires phosphatidylinositol 3-OH-kinase signaling. Am J Physiol Endocrinol Metab 289, E1051–1057, doi:10.1152/ajpendo.00094.2005 (2005). [PubMed: 16046456]
27. McRae PA, Rocco MM, Kelly G, Brumberg JC & Matthews RT Sensory deprivation alters aggrecan and perineuronal net expression in the mouse barrel cortex. J Neurosci 27, 5405–5413, doi:10.1523/JNEUROSCI.5425-06.2007 (2007). [PubMed: 17507562]
28. Nakamura M et al. Expression of chondroitin sulfate proteoglycans in barrel field of mouse and rat somatosensory cortex. Brain Res 1252, 117–129, doi:10.1016/j.brainres.2008.11.022 (2009). [PubMed: 19056358]
29. Dityatev A et al. Activity-dependent formation and functions of chondroitin sulfate-rich extracellular matrix of perineuronal nets. Dev Neurobiol 67, 570–588, doi:10.1002/dneu.20361 (2007). [PubMed: 17443809]
30. Luquet S, Perez FA, Hnasko TS & Palmiter RD NPY/AgRP neurons are essential for feeding in adult mice but can be ablated in neonates. Science 310, 683–685, doi:10.1126/science.1115524 (2005). [PubMed: 16254186]
31. Xu J et al. Genetic identification of leptin neural circuits in energy and glucose homeostases. Nature 556, 505–509, doi:10.1038/s41586-018-0049-7 (2018). [PubMed: 29670283]
32. de Winter F et al. The Chemorepulsive Protein Semaphorin 3A and Perineuronal Net-Mediated Plasticity. Neural Plast 2016, 3679545, doi:10.1155/2016/3679545 (2016). [PubMed: 27057361]
33. Barker DJP Fetal and Infant Origins of Adult Disease. (British Medical Journal, 1992).
34. Ravelli GP, Stein ZA & Susser MW Obesity in young men after famine exposure in utero and early infancy. N Engl J Med 295, 349–353, doi:10.1056/NEJM197608122950701 (1976). [PubMed: 934222]
35. Ravelli AC et al. Glucose tolerance in adults after prenatal exposure to famine. Lancet 351, 173–177 (1998). [PubMed: 9449872]
36. Vickers MH et al. Neonatal leptin treatment reverses developmental programming. Endocrinology 146, 4211–4216, doi:10.1210/en.2005-0581 (2005). [PubMed: 16020474]
37. Miyata S & Kitagawa H Formation and remodeling of the brain extracellular matrix in neural plasticity: Roles of chondroitin sulfate and hyaluronan. Biochim Biophys Acta 1861, 2420–2434, doi:10.1016/j.bbagen.2017.06.010 (2017).
38. Saghatelyan AK et al. Reduced perisomatic inhibition, increased excitatory transmission, and impaired long-term potentiation in mice deficient for the extracellular matrix glycoprotein tenascin-R. Mol Cell Neurosci 17, 226–240, doi:10.1006/mcne.2000.0922 (2001). [PubMed: 11161481]
39. Hylin MJ, Orsi SA, Moore AN & Dash PK Disruption of the perineuronal net in the hippocampus or medial prefrontal cortex impairs fear conditioning. Learn Mem 20, 267–273, doi:10.1101/lm.030197.112 (2013). [PubMed: 23592037]

40. Thaler JP et al. Obesity is associated with hypothalamic injury in rodents and humans. The Journal of clinical investigation 122, 153–162, doi:10.1172/JCI59660 (2012). [PubMed: 22201683]

41. Douglass JD, Dorfman MD, Fasnacht R, Shaffer LD & Thaler JP Astrocyte IKKbeta/NF-kappaB signaling is required for diet-induced obesity and hypothalamic inflammation. Molecular metabolism 6, 366–373, doi:10.1016/j.molmet.2017.01.010 (2017). [PubMed: 28377875]

42. Valdearcos M et al. Microglial Inflammatory Signaling Orchestrates the Hypothalamic Immune Response to Dietary Excess and Mediates Obesity Susceptibility. Cell metabolism 26, 185–197 e183, doi:10.1016/j.cmet.2017.05.015 (2017). [PubMed: 28683286]

43. Balland E et al. Hypothalamic tanycytes are an ERK-gated conduit for leptin into the brain. Cell metabolism 19, 293–301, doi:10.1016/j.cmet.2013.12.015 (2014). [PubMed: 24506870]

44. Gao Y et al. Hormones and diet, but not body weight, control hypothalamic microglial activity. Glia 62, 17–25, doi:10.1002/glia.22580 (2014). [PubMed: 24166765]

Methods References

45. Tamamaki N et al. Green fluorescent protein expression and colocalization with calretinin, parvalbumin, and somatostatin in the GAD67-GFP knock-in mouse. J Comp Neurol 467, 60–79 (2003). [PubMed: 14574680]

46. Leshan RL, Bjornholm M, Munzberg H & Myers MG Jr. Leptin receptor signaling and action in the central nervous system. Obesity 14 Suppl 5, 208S–212S, doi:10.1038/oby.2006.310 (2006). [PubMed: 17021368]

47. Madisen L et al. A robust and high-throughput Cre reporting and characterization system for the whole mouse brain. Nat Neurosci 13, 133–140, doi:10.1038/nn.2467 (2010). [PubMed: 20023653]

48. van den Pol AN et al. Neuromedin B and gastrin-releasing peptide excite arcuate nucleus neuropeptide Y neurons in a novel transgenic mouse expressing strong Renilla green fluorescent protein in NPY neurons. J Neurosci 29, 4622–4639, doi:10.1523/JNEUROSCI.3249-08.2009 (2009). [PubMed: 19357287]

49. Cowley MA et al. Leptin activates anorexigenic POMC neurons through a neural network in the arcuate nucleus. Nature 411, 480–484, doi:10.1038/35078085 (2001). [PubMed: 11373681]

50. Mirzadeh Z, Doetsch F, Sawamoto K, Wichterle H & Alvarez-Buylla A The subventricular zone en-face: wholemount staining and ependymal flow. J Vis Exp, 10.3791/1938 (2010).

51. Doetsch F, Garcia-Verdugo JM & Alvarez-Buylla A Cellular composition and three-dimensional organization of the subventricular germinal zone in the adult mammalian brain. J.Neurosci 17, 5046–5061 (1997). [PubMed: 9185542]

52. Hawrylycz MJ et al. An anatomically comprehensive atlas of the adult human brain transcriptome. Nature 489, 391–399, doi:10.1038/nature11405 (2012). [PubMed: 22996553]

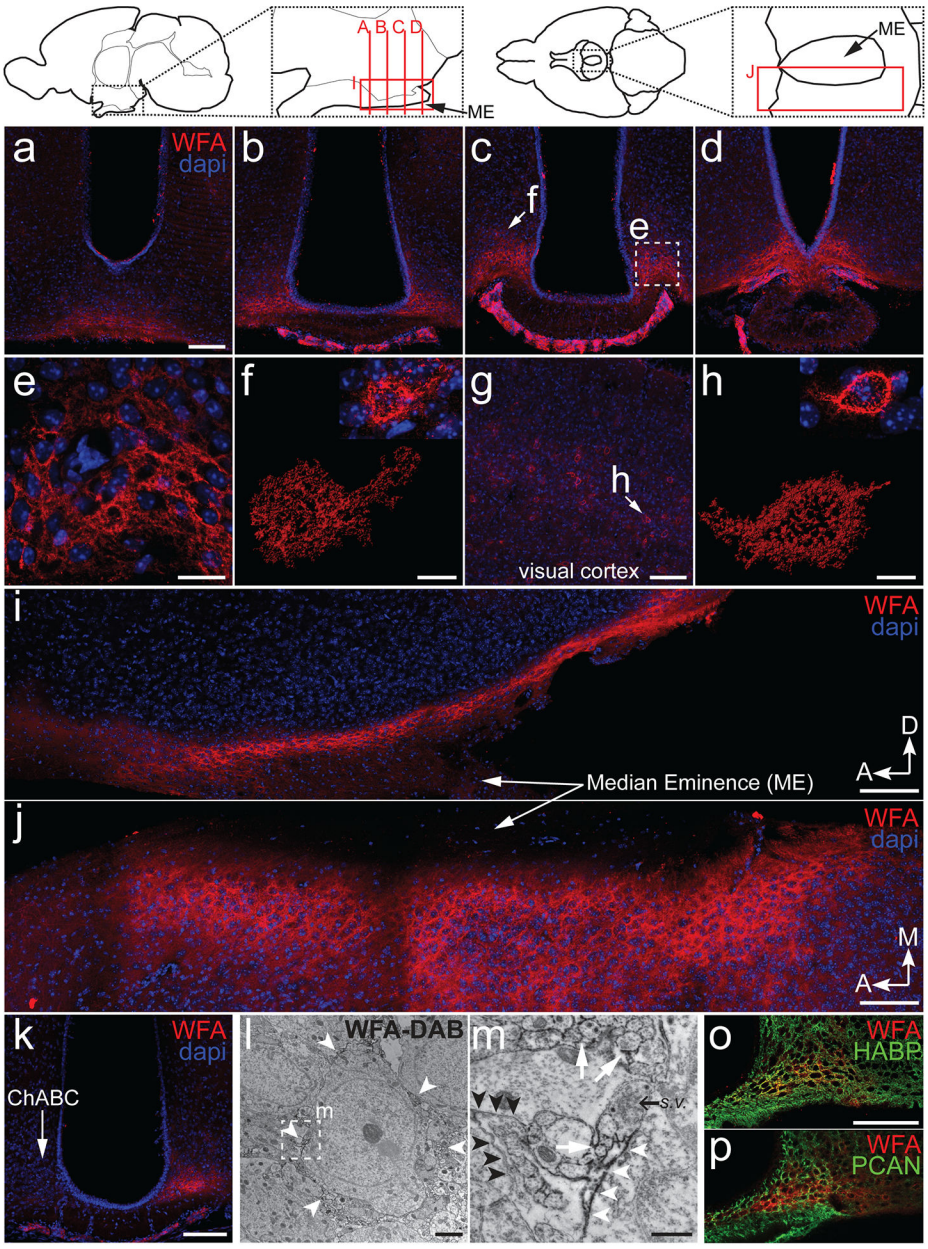

Figure 1.

Wisteria Floribunda agglutinin (WFA)-labeling in the ventromedial ARC forms a "collar" around the ME. Diagrams at top show mid-sagittal view (left) and ventral view (right) of the mouse brain with insets showing the location and orientation of panel images.

(a-d) WFA-labeled (red) coronal sections through the Arc, starting just rostral to and progressing through the ME, show a concentration of WFA-labeled cells located in the ARC at its junction with the ME. Note that the very intense staining below the ME does not correspond to labeling around neurons, but to the pia around the ME.

(e) Higher magnification image of the boxed region in (c) showing the dense cluster of WFA-labeled ARC cells.

(f) High magnification Imaris 3-dimensional rendering of an isolated WFA-labeled cell at the periphery of the dense cluster (arrow in c) reveals that WFA labels the soma and proximal processes of ARC cells. Inset shows the raw image.
(g-h) Low (g) and high (h) magnification images of PNNs labeled by WFA in the visual cortex, where they have been extensively studied, for comparison. Note similar PNN pattern between (h) and (f) wrapping the soma and proximal process.
(i-j) WFA-labeled wholemounts of the ARC viewed from the 3rd ventricle wall en-face (i) or the ventral brain surface (j) reveal the distribution of labeled ARC cells forming a "collar" around the ME, which does not contain labeling. From the ventricular surface view (i), the WFA-labeled ARC cells appear as a continuous band along the ventral margin of the ARC.
(k) WFA-labeled coronal section from a wild-type mouse sacrificed 2 days after stereotactic unilateral intra-Arc injection of Chondroitinase ABC, an enzyme that digests chondroitin sulfate carbohydrates.
(l) Low-power electron micrograph of an ARC section labeled with WFA-DAB shows electron dense DAB deposits surrounding a single ARC neuron (white arrowheads).
(m) High-power electron micrograph corresponding to the boxed region in (l) shows WFA-labeling localized to the membrane around the cell soma (white arrowheads) and neurites (white arrows). Note labeling adjacent to an apparent terminal filled with synaptic vesicles (s.v.), as well as the appearance of non-labeled membranes (black arrowheads).
(o-p) Confocal images of coronal sections through the ARC stained for other PNN components, including hyaluronic acid using HABP (o, green) and the chondroitin sulfate proteoglycan phosphacan (p, green), show colocalization with WFA (red) in the ARC, providing evidence that ARC WFA-labeling corresponds to PNNs.
Scale bars: 100 um (a-d, g, i-k, o-p), 20 um (e), 10 um (f, h), 2 um (l), 500 nm (m). Images in (a-h), (i-j), (k), (l-m), and (o-p) are representative of data from 10, 6, 5, 4, and 3 animals, respectively.

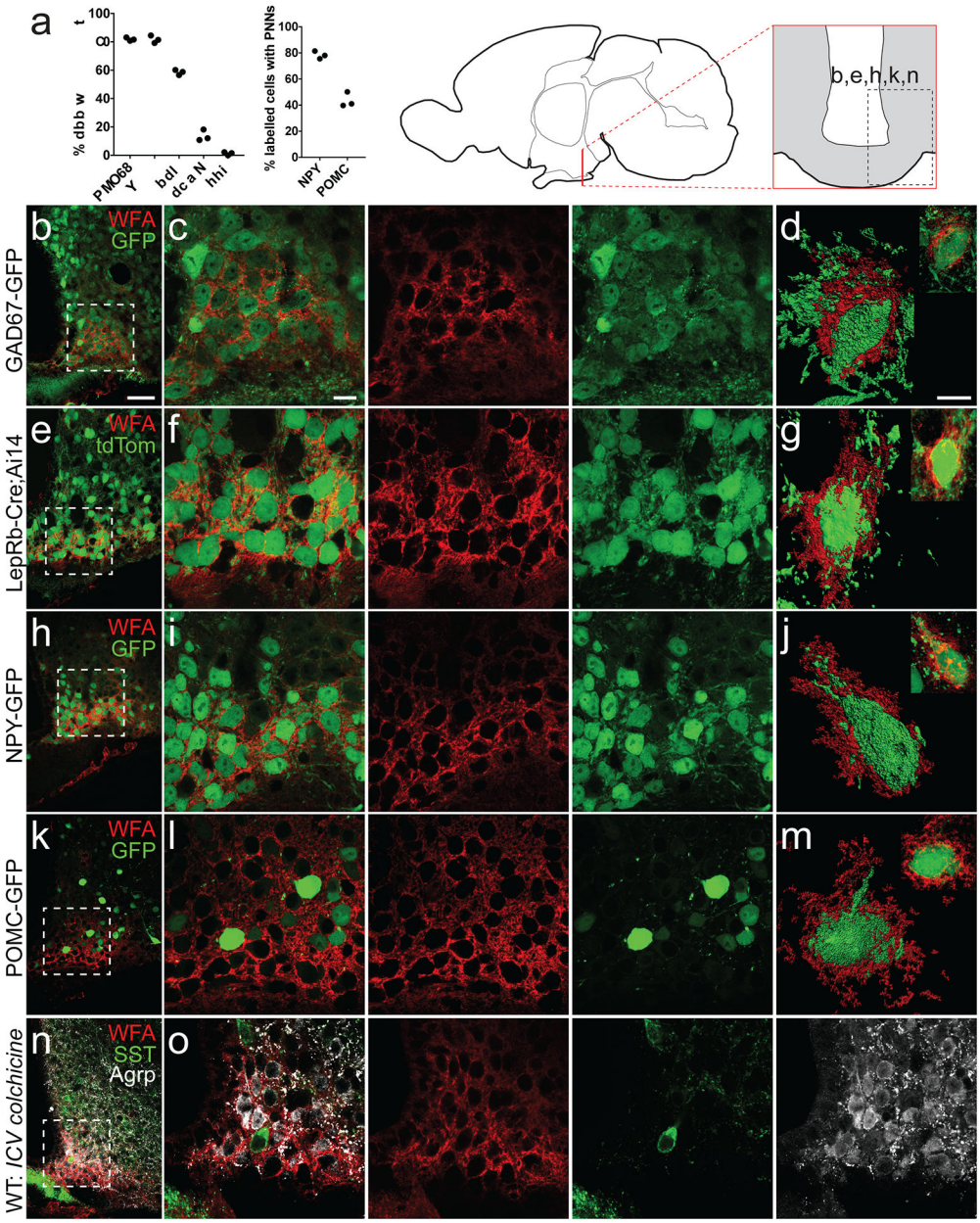

Figure 2.

PNNs enmesh GABAergic, LepRb-positive, Agrp/NPY neurons in the Arc. Diagram at top shows mid-sagittal view of mouse brain with location and orientation of panel images.

(a) Dot plots show the proportion of individual neuronal subtypes enmeshed by PNNs. Dots in this and all subsequent dot plots represent data from independent animals (n=3 animals for each neuronal subtype studied). The left plot shows the percentage of all PNN-enmeshed ARC cells that belong to a particular neuronal subtype. The right plot shows the percentage of all ARC Npy-GFP or POMC-GFP cells that are enmeshed by PNNs.

Low (b, e, h, k, n) and high (c, f, i, l, o) magnification images of coronal sections stained with WFA (red) and antibodies to GFP (green) (b, h, k), dsRed (green) (e), or SST (green) and Agrp (white) (n) show that most PNN-enmeshed cells are GAD67-GFP-positive

(GABAergic), LepRb-positive, and NPY-positive, while few enmeshed cells express POMC or SST.

(d, g, j, m) High magnification Imaris 3-dimensional surface rendering of isolated ARC PNN-enmeshed cells belonging to the various neuronal subtypes (corresponding to b, e, h, k, respectively) show PNNs wrapping the soma and proximal processes. Insets show raw images. See corresponding supplementary movies 1 and 3 for (d) and (j), respectively. Scale bars: 50 um (b, e, h, k, n), 20 um (c, f, i, l, o), 10 um (d, g, j, m). Images in (b-d), (e-g), (h-j), (k-m), and (n-o) are representative of data from 3 GAD67-GFP mice, 3 LepRb-Cre;Ai14 mice, 3 NPY-GFP mice, 3 POMC-GFP mice, and 3 C57B/6 mice injected with ICV colchicine, respectively.

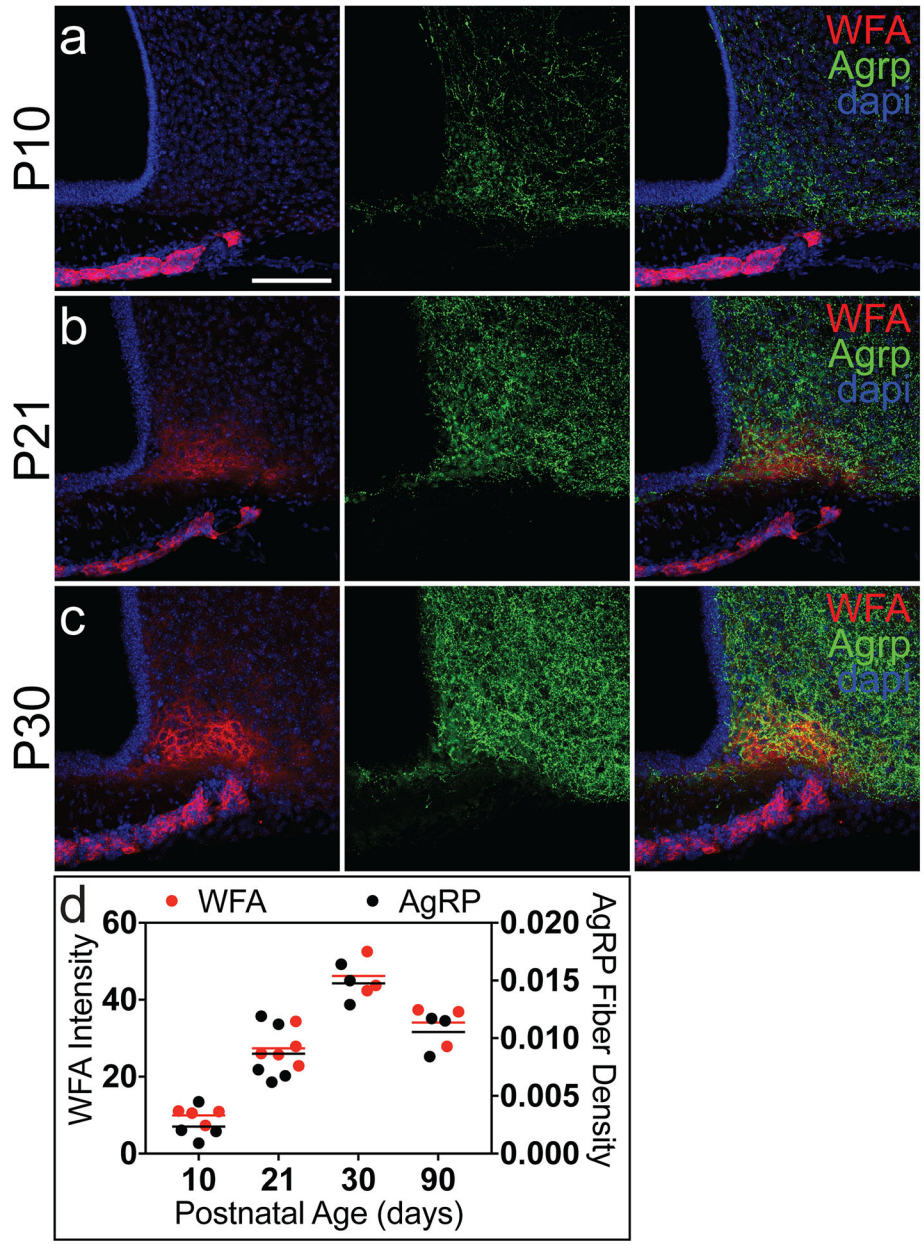

Figure 3.

PNN formation in the ARC occurs during the lactation and periweaning period, corresponding with the maturation of Agrp neurons.

(a-c) Confocal images of coronal sections stained with WFA (red), Agrp (green), and dapi (blue) from postnatal wild-type mice at age P10 (a), P21 (b), and P30 (c). PNN staining intensity and ARC Agrp fiber density increase in parallel over this time period.

(d) Dot plot shows correlated increase in WFA intensity and Agrp fiber density in the ARC from P10 to P30, as well as at P90. Dots (WFA intensity in red, Agrp density in black) represent values from independent animals (n=4 (P10); 5 (P21); 3 (P30); and 3 (P90)), and horizontal bars represent the mean. WFA intensity is represented by the average over all

voxels in the ARC region of interest, with range 0–255. Agrp fiber density is measured as the volume of Agrp+ voxels divided by the total volume of the ARC region of interest. Scale bar: 100 um (a-c). Images in (a), (b), and (c) are representative of data from 4, 5, and 3 animals, respectively.

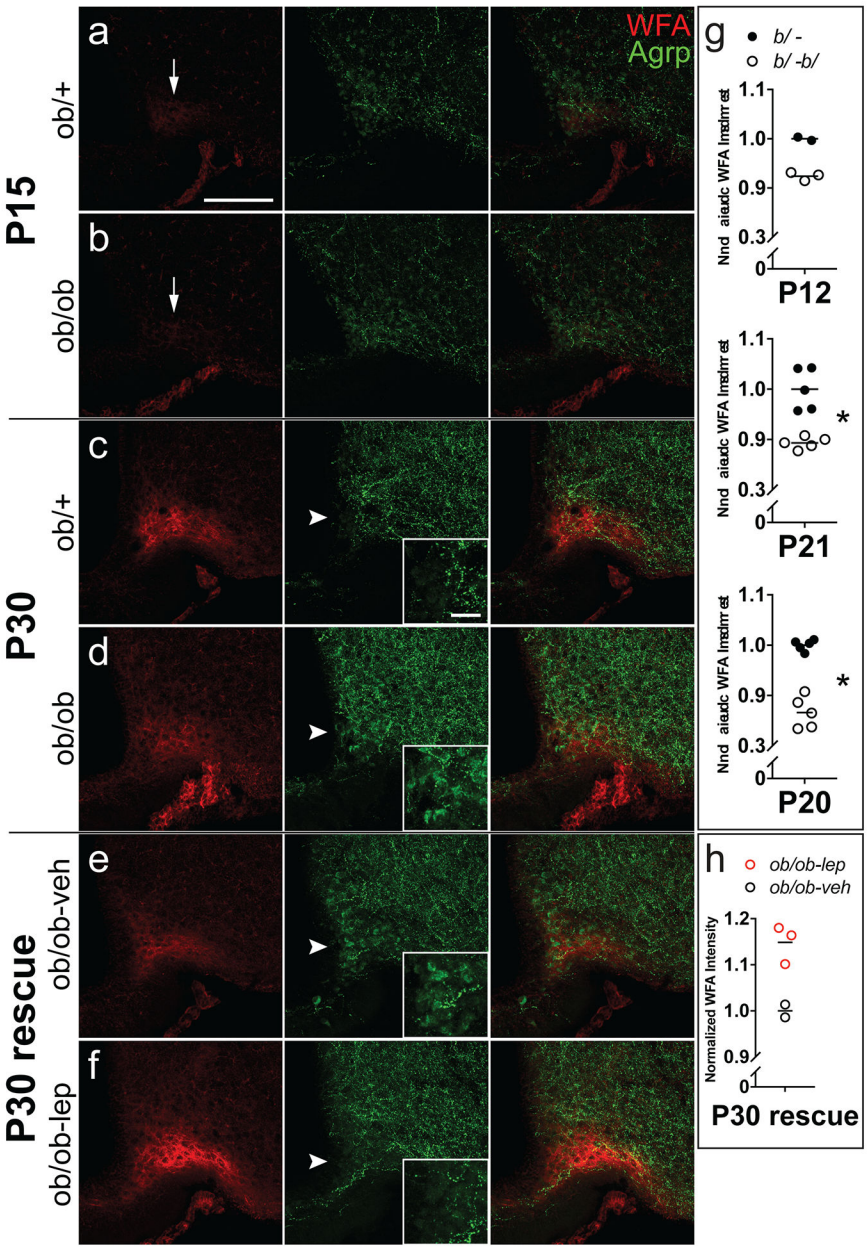

Figure 4.

Leptin-deficient *ob/ob* mice have impaired PNN formation during postnatal development that can be rescued by leptin administration during the critical period.

(a-d) Confocal images of ARC sections from *ob/ob* (b,d) and *ob/+* (a,c) control littermates at P15 (a,b) and P30 (c,d), stained with WFA (red) and Agrp (green), show reduced WFA labeling and apparent disruption of PNN architecture in the ARC. Arrows in (a,b) indicate the ARC region where the earliest PNN formation is seen at P15 in *ob/+* mice, but not in *ob/ob* littermates. Images in (a), (b), (c), and (d) are representative of data from 2, 3, 5, and 5 animals, respectively.

(e-f) Confocal images of ARC sections from *ob/ob* pups that received daily i.p. injections of leptin (f) or vehicle (e) from P10 to P30 before being euthanized for analysis with WFA

(red) and Agrp (green). Leptin administration during this critical period appeared to restore WFA labeling intensity and PNN architecture. Insets in (c-f) show higher magnification of the ventromedial ARC region indicated by the arrowhead, revealing an increase in Agrp expression within neuronal soma in leptin deficiency. Images in (e) and (f) are representative of data from 2 and 3 animals, respectively.

(g-h) Dot plots show normalized intensity values for WFA in the ARC of P15, P21, and P30 *ob/+* (filled circles) and *ob/ob* (open circles) mice (g), or P30 *ob/ob* mice treated from P10 onward with daily i.p. leptin (red open circle) or vehicle (black open circle) injection (h). Values were normalized to the mean WFA intensity of the control groups (*ob/+* or *ob/ob-*veh). Dots represent values from independent animals (n= 2 *ob/+* and 3 *ob/ob* (P15); 5 *ob/+* and 5 *ob/ob* (P21); 5 *ob/+* and 5 *ob/ob* (P30); 2 *ob/ob-veh* and 3 *ob/ob-lep* (P30 rescue)). Horizontal bars represent the mean. There was a consistent decrease in ARC PNN intensity across multiple postnatal ages in *ob/ob* mice compared to their *ob/+* littermates, which appeared to be restored in *ob/ob* mice at P30 by leptin administration during the critical period (*P21 *ob/ob* 0.89±0.01 vs. *ob/+* 1.00±0.02, two-tailed t-test p=0.0005, t=5.545, df=8, 95% CI of difference: −0.151 to −0.062; P30 *ob/ob* 0.87±0.01 vs. *ob/+* 1.00±0.01, two-tailed t-test p=0.0001, t=8.975, df=8, 95% CI of difference: −0.168 to −0.099).

Scale bars: 100 um (a-f), 20 um (insets in c-f).